The Real-Time, High-Resolution X-Ray Video Microscopy of Solidification in Aluminum Alloys

Lars Arnberg and Ragnvald H. Mathiesen

Enhanced for the Web

Read this article on the *JOM* web site (www.tms.org/JOMPT) to see video sequences of solidification in aluminum alloys.

The directional solidification of thin alloy sheets in a Bridgman furnace has been studied by x-radiography using high-brilliance synchrotron x-radiation in combination with a low-noise, fast-readout camera. Spatial resolutions down to 1.5 μm and a temporal resolution of about 0.15 s have permitted real-time video microscopy of microstructural evolution during columnar and equiaxed dendrite growth and eutectic and monotectic growth. The technique has also allowed for direct observations of important solidification phenomena such as dendrite fragmentation and porosity formation, primarily in aluminium alloys. As a result, insights have been gained into mechanisms of dendrite fragmentation, criteria for dendrite tip kinetics and interface stability during transient growth, and microstructure formation mechanisms during monotectic solidification. The results are expected to be important for validation of dendrite growth models. This paper presents a review of the technique as well as examples of images obtained during solidification of aluminum alloys.

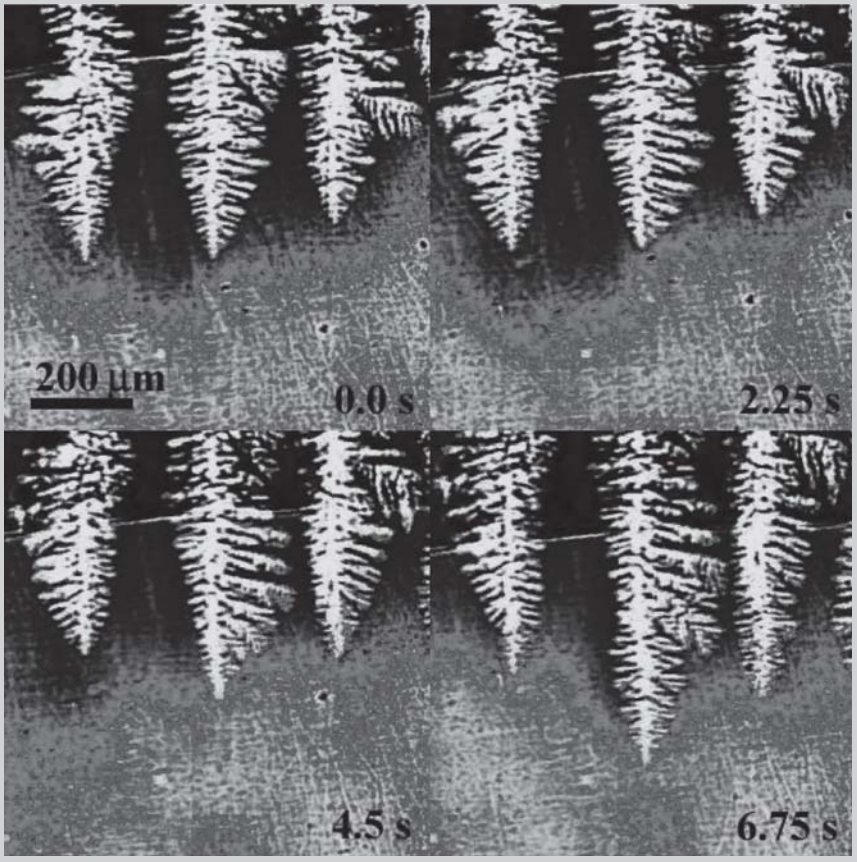

WEB

Figure 1. Columnar dendritic and planar eutectic growth in Al-30Cu. G = 27 K/mm, v = –22.5 μm/s. *[See animation on-line.]*

INTRODUCTION

The final microstructures and properties of castings depend to a large extent on the thermodynamics and kinetics of the solidification process. Accordingly, there is strong industrial and academic motivation for a better understanding of and control over the fundamental aspects of solidification.

Over recent decades, advanced modelling has evolved to cover many aspects of solidification science, from predicting the morphology of growing dendrites in two or three dimensions (2-D or 3-D) and important phenomena such as porosity and segregation to the numerical modelling of real casting processes—spanning length scales from the atomic to the macroscopic. While computer simulations have been firmly established on all levels, the provision of new experimental data to guide theory and modelling and assist in their refinement has fallen behind. In particular there is a gap to bridge in devising experimental methods for in-situ observations of metal and alloy solidification microstructures and phenomena allowing for proper assessment of kinetics.

Experimental methods that have traditionally been used to investigate how microstructures of metals develop during solidification include metallographic investigations of alloys, either ex-situ after a completed solidification or with alloys that have been quenched or

decanted during solidification. Transparent organic materials with low melting points and solidification entropies have been used extensively as analog systems that can be studied in-situ under the microscope. All these methods have, however, significant shortcomings in providing information about the dynamics of metal solidification.[1]

Metal transparency and interaction with x-rays constitute candidate principles from which methods for in-situ monitoring of solidification processes could be constructed. However, source brightness and detection efficiency has limited the practical impact of x-rays as diagnostic tools for studies at physically relevant time and length scales (i.e., milliseconds and micrometers). The first x-ray investigations were based on radiography with conventional sources and used for in-situ studies of solute redistribution and boundary layer propagation.[2,3] The geometrical resolutions obtained, $\Delta r_g >$ 50 μm, prevented studies with curved fronts, but the resolution by contrast was adequate to verify proximity to Scheil conditions. In their early work M.P. Stephenson and J. Beech[3] demonstrated the influence of buoyancy convection on the solute boundary layer by comparative measurements varying the growth direction relative to gravity. In the following years, little progress was made. In the mid-1990s, micro-focus sources were introduced in solidification science by a series of successive studies of striations, droplet formations, and engulfment in binary monotectics,[4,5] reporting $\Delta r_g \sim$ 30 μm. A similar setup was used at that time to study convection and solidification microstructures in Ga-In.[6]

The major challenge with conventional sources was and still is to obtain adequately high flux at the sample to facilitate short acquisition times that limit contrast blurring by the temporal evolution of the system. Another problem is the substantially lower resolution obtained with curved fronts (e.g., close to or at dendrite tips, which due to their 3-D curvature fade as absorption contrast objects). Improvements in x-ray detectors combined with the eminent brightness and collimation offered by third-generation synchrotron radiation (SR) sources have enabled the use of x-ray imaging-based techniques to investigate the interface morphology evolution, solute transport, and various process phenomena at spatiotemporal resolutions gradually approaching those of video microscopy.

In general, there are three different viable imaging techniques for the real-time investigation of solidification microstructures in alloys: 2-D x-ray radiography, 2-D white-beam x-ray topography, and ultra-fast 3-D x-ray tomography. Ultra-fast SR x-ray tomography with approximately 10 s acquisition per tomogram and a $\Delta r_g \sim 3$ μm resolution limit has recently been demonstrated as a promising tool in solidification science.[7] However, a 10 s acquisition requires the microstructure to remain semi-stationary within resolution limits during exposure of the underlying radiographic sequence. It is therefore most suited for studies of late-stage phenomena occurring after network coherency is established, and by employing low cooling rates so that the morphology evolution takes place over time scales of several seconds to minutes. Ultra-fast tomography has been used to obtain detailed 3-D information on deep-in mushy zone processes like ripening and low-permeability melt feeding.[7] In general, tomography is less versatile than the other methods as observations are indirect, being available only after a computer reconstruction of the 3-D object. White-beam topography has been used quite extensively to study solidification microstructures,[8–11] its main advantage being supreme solid-liquid (s-l) interface contrast by phase-selective diffraction from the solid. It also offers unique capabilities for direct studies of momentum transfer at the s-l interface.[11] However, in-situ topography is limited by the output signal strength; typically obtainable spatiotemporal resolutions are on the order of 15 μm and 2 s.

The most flexible technique for spatiotemporal imaging of evolving solidification microstructures is x-radiography, provided that the alloy system under investigation contains segregates that can be resolved by transmission contrast. With third-generation SR sources, partial

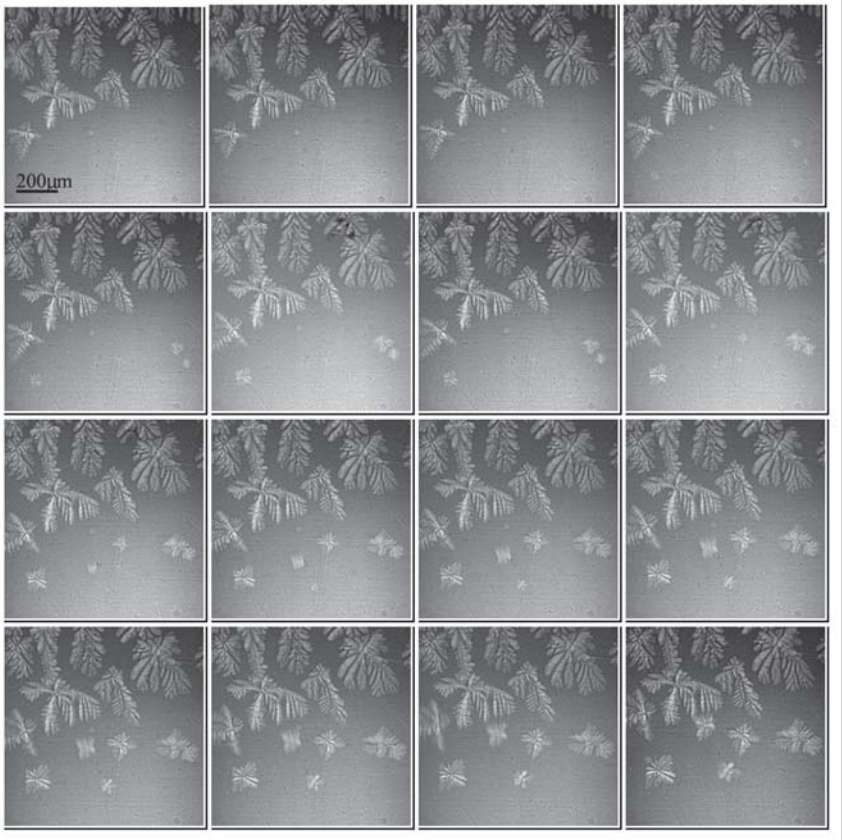

WEB

Figure 2. Equiaxed dendritic growth in Al-20Cu. G = 38 K/mm, v = 17.5 μm/s. *[See animation on-line.]*

beam coherence can be obtained at high photon energies, facilitating the use of x-ray phase contrast[1,12] in addition to the more conventional photoelectric absorption contrast. In general, this leads to contrast enhancement at the s-l interface, and also enables studies of s-l interfaces between aggregates of similar atomic compositions. The first demonstration of in-situ SR radiography in solidification science was carried out with various alloys from the Sn-Pb system.[13] Cellular, columnar, and equiaxed dendritic microstructures were studied employing a high-resolution fast readout detector[14] equipped with specially developed components for high-resolution time-resolved imaging. In successive applications of the setup, solidification microstructures and phenomena were studied in various alloys from the Al-Cu system,[1,15–17] where nominal resolutions combined to an optimum $\Delta r_{tg} \sim 1.5\ \mu m$ at the s-l interface. Recently, other groups have applied similar setups to study solidification in Sn-Bi[18–20] and Al-Ni.[21–23]

The new high-resolution in-situ imaging techniques have provided new quantitative morphological, solutal, and kinetic data on solidification microstructure development. Another important benefit of the technique is real-time video microscopy of solidification sequences, which can provide a conceptual understanding of the dynamics of metal solidification processes that no other method has been able to.

This article will review some recent high-resolution x-ray imaging work on aluminum alloys, with supplemental video sequences available on-line.

See the sidebar on page 24 for experimental procedures.

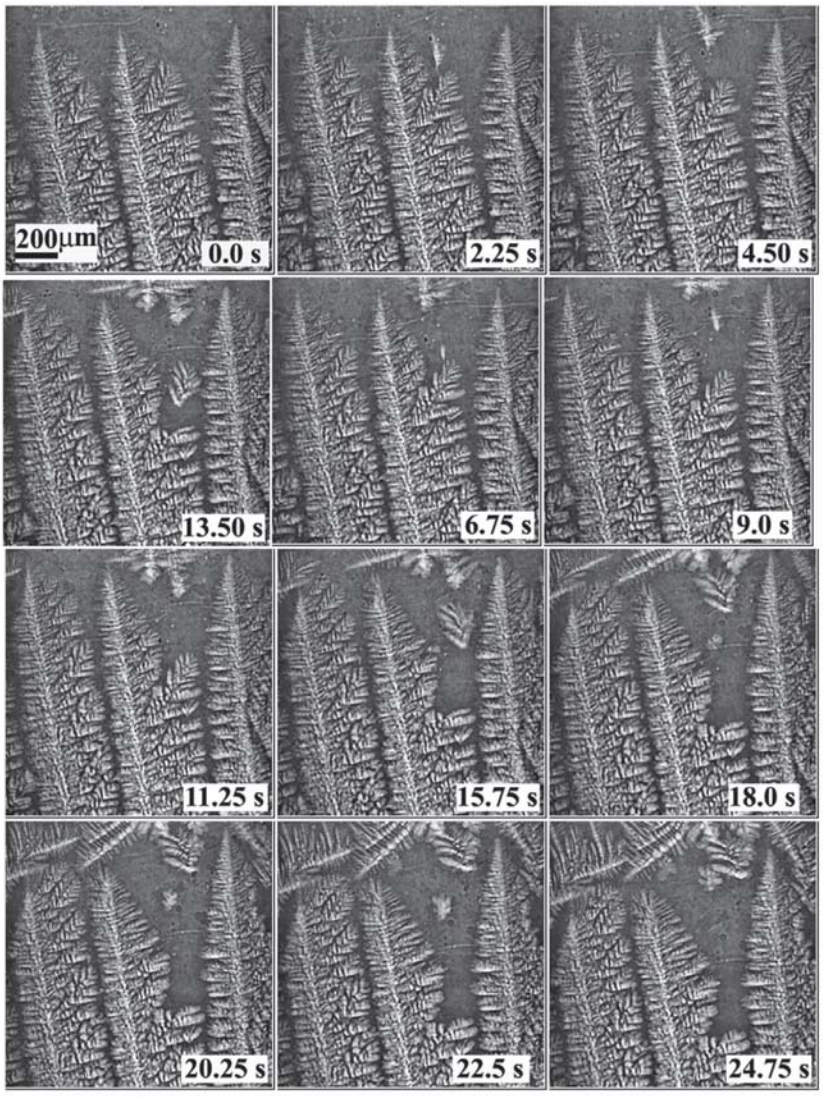

WEB

Figure 3. Fragmentation in Al-20Cu. G = 48 K/mm, v = 25 µm/s. *[See animation on-line.]*

RESULTS AND DISCUSSION

Columnar Growth in Al-Cu

Figure 1 shows columnar dendritic and eutectic growth in Al-30Cu (all compositions are in weight percent) directionally solidified with the temperature gradient parallel to gravity. The composition is close to the Al-Cu eutectic at 33 wt.% and the eutectic front appears as a near-horizontal line across the images, mainly visible due to phase contrast. At the dendritic s-l interface both phase shift and absorption contributes to the contrast. The absorption contrast available also allows for a direct visualization of the solute field in the liquid ahead of the dendrites. The mesoscopic variations in this solute field are due to settling melt flows pluming out of the interdendritic columns into the liquid region ahead of the columnar front. The melt flow promotes local destabilizations of the solute boundary layer forming ahead of the s-l interface, causing the different dendrite tips to grow with velocities that alternate in a sinusoidal manner about an approximately constant eutectic front velocity. The images illustrate the difficulties of achieving steady-state growth, mainly due to the presence of thermosolutal flow in a manner that is in good agreement with results from 2-D phase-field simulations of a similar case.[24] There is also most likely a small contribution to the unstable growth conditions from a long-term sample position dependent drift in the furnace-to-sample heat transfer.[15]

Image processing allows the extraction of quantitative and spatiotemporally resolved data from the image sequence on the solute concentration field in the liquid and on the morphology of the s-l interface.[15] The morphological data extracted from the sequence of Figure 1 has also been used for qualitative comparison with dendritic tip stability calculations.[25] Also, S. Boden and coworkers demonstrated that liquid flow velocity fields can be made available

from processing this type of radiographic image sequence.[26]

Equiaxed Growth in Al-Cu

Figure 2 shows equiaxed growth in an Al-20Cu alloy that has been inoculated by the addition of a grain-refining Al-Ti-B master alloy corresponding to 25 ppm titanium and 5 ppm boron. New aluminum grains nucleate more or less continuously in the melt. A fraction of the crystals also nucleates from seeds that stick to the oxide skin formed on the exterior of the sample metal sheet. The crystals that form on the walls are easily distinguished from those that nucleate freely in the melt due to the strong buoyancy exerted on the latter category, from the parent melt which at C_0 has a density that is ~1.4 times that of the α-Al crystals. Since solidification is parallel to gravity, the upward motion of the crystals is stopped as a coherent network is established. Complex thermosolutal flow is present also in this sequence, visible as horizontal components in the trajectories of the individual dendrites.

Dendrite Fragmentation and Columnar-to-Equiaxed Transition

The solidification direction in Figures 1 and 2 was parallel to gravity. In experiments where columnar crystals grew upward, antiparallel to gravity, the dendrites often fragmented and sometimes these fragments survived. Figure 3 shows dendrite fragmentation in an Al-20Cu alloy.[27,28] The fragmentation in this material can be attributed to the heavier solute that is rejected from the tip and flows into the mush, causing ternary arms to melt at their root. Since this occurs close to the front, the fragments can be transported by buoyancy forces out of the highly permeable

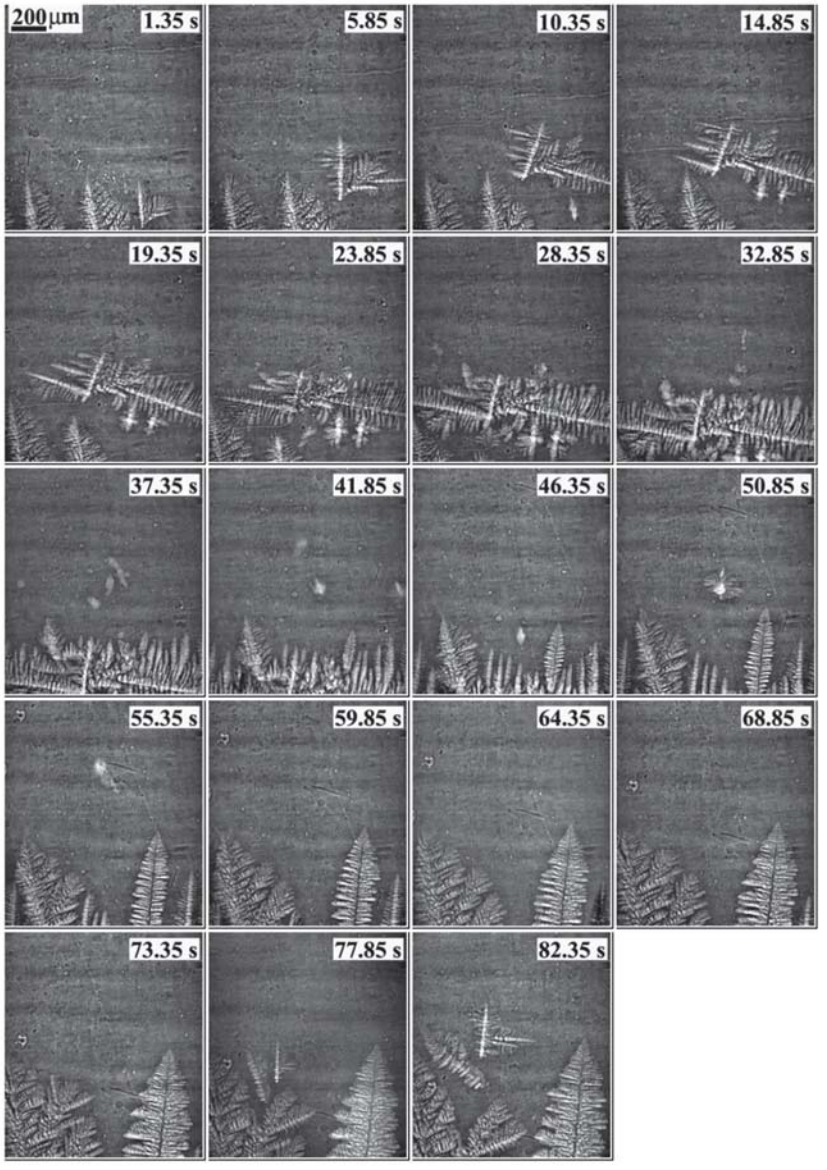

WEB

Figure 4. Fragmentation and initiation of CET in Al-20Cu. G = 48 K/mm, v = 25 μm/s. *[See animation on-line.]*

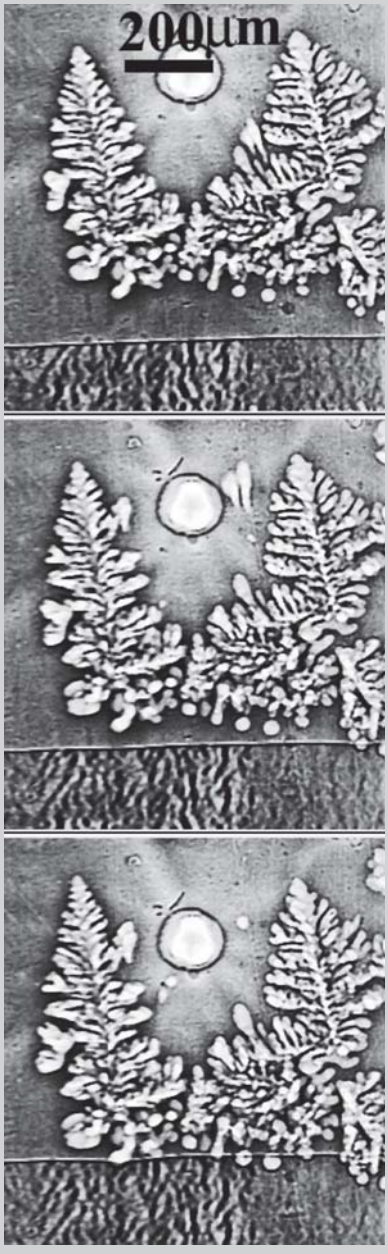

WEB

Figure 5. Dendrite fragmentation during recalescence from solidifying eutectic in an Al-30Cu alloy. G = 15 K/mm, v = 5 μm/s. *[See animation on-line.]*

mush. When the fragments reach into the constitutionally undercooled region close to and ahead of the columnar front, they grow by consumption of the local solvent. Consequently, even more solute is accumulated along the trajectory of the initial fragment, which settles into the interdendritic column causing a cascade of secondary fragments detaching in the wake of the initial one. It is worth noting that while the initial fragment clearly grew dendritically during flow, the secondary fragments do not show similar growth. This can be taken as evidence that the local undercooling has been swept away by the growth of the first fragment. When the first fragment reaches into the liquid region ahead of the columnar front, it grows sufficiently large to cause solute accumulation ahead of the front that settles into the neighboring interdendritic regions and causes detachment to occur here as well. Eventually this cascade of secondary fragmentation spreads laterally across the field-of-view and the columnar front is completely blocked from further growth, both mechanically and solutally, since the liquid undercooling ahead of the columnar front is swept away. In Figure 4 the same sample has been solidified once more with exactly the same parameter setting, except that the field of view is shifted slightly upward.[27] Once again fragmentation is initiated by solute pile-up, eventually leading to a blocking of the columnar front, and as seen toward the end of this sequence where a new columnar front is hindered from stabilizing by a second cycle of detachments. The initial blocking of the columnar front and the irregular microstructures that form afterward are believed to represent the initial stages of a columnar-to-equiaxed transition (CET), found to occur in many castings.

Figure 5 shows another mechanism for dendrite detachment, recalescence in Al-30Cu. As a eutectic front approaches the dendrites, the latent heat of fusion released by the eutectic front causes local remelting and detachment of dendrite arms. This would normally happen in the region close to secondary solidification fronts, like the eutectic, and therefore, in systems with a lower alloying would occur too deep into the mush to allow for transport of the fragments out of the mush and initiate a CET.[27]

Eutectic Solidification

Figure 6 shows planar eutectic growth in Al-30Cu. This is the same alloy as in Figure 1, but the temperature gradient has been increased and the growth rate decreased so that the front is no longer constitutionally undercooled.[1] Steady-state conditions seem to prevail since the position of the front is stationary and growth occurs at a constant temperature. Figure 7 shows the same alloy, but here the growth rate has been increased from 7 μm/s to 32 μm/s (a high temperature gradient has been retained) which has destabilized the front into eutectic cells and dendrites.

Hydrogen Porosity

Some aluminum samples were found to contain sufficient hydrogen to promote bubble formation during solidification. Figure 8 shows how such bubbles form porosity in Al-30Cu.[1] Solidification in this sample is parallel with gravity and the solidification front prevents the bubbles from escaping by flotation. The formation of the bubbles can not be seen in the sequence; they probably nucleate well ahead of the solidification front outside the field of view, but the incorporation into the eutectic front can be seen and results in elongated pores.

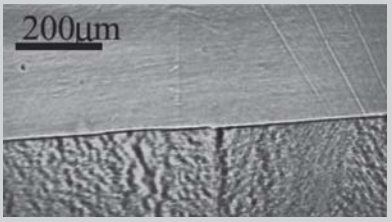

Figure 6. Planar eutectic solidification in Al-30Cu. G = 46 K/mm, v = 6.4 μm/s. *[See animation on-line.]*

Phase Separation during Monotectic Solidification

Figure 9 shows droplet formation, motion, and coagulation and monotectic solidification in hypermonotectic Al-6Bi (the monotectic composition is at about 4 wt.% Bi).[29] In the hypermonotectic systems a liquid-liquid phase separation into an aluminum-rich primary melt engulfing droplets of a secondary bismuth-rich liquid phase is expected ahead of the monotectic reaction, with a slight increase of the element segregation between the two liquid phases as the temperature approaches the monotectic reaction where α-Al solidifies. When the secondary phase droplets or embryos are adequately small they exert Brownian motion, but as their size increases they will be set in collective motion by a combination of external forces.

First, gravity acts as an external force since the bismuth droplets are about 3.5 times denser than the primary melt. Second, Marangoni forces arise due to the thermal and/or solutal dependence of the liquid-liquid surface tension, promoting primary melt flow around the droplets toward the region of the highest surface tension. Thus, in a temperature gradient, the Marangoni flow of the droplets would be parallel to the gradient. Finally, for viscous flow a Stokes drag is exerted on the moving droplets by the surrounding liquid.

In the case shown here, with solidification antiparallel to gravity, the thermal Marangoni force and gravity will be directed oppositely, and since the former scales with the surface of the droplet while the latter scales with its volume,

EXPERIMENTAL PROCEDURES

The solidification experiment as well as the imaging technique have been described extensively elsewhere[1,15] and only a short review will be given here. A Bridgman-type solidification furnace has been utilized in all experiments. In this experiment, a thin (0.1–0.2 mm) alloy sample is placed in the gap between two furnaces, one at a temperature above the liquidus and the other below the solidus. The furnace temperatures and gap and thus the temperature gradient can be regulated independently. The sample is translated by a stepping motor. The solidification allows for experiments parallel (downward) or antiparallel (upward) to gravity. The sample is contained in a quartz glass envelope and protected from reaction with the glass by a thin layer of boron nitride spray. All experiments have been carried out at the European Synchrotron Radiation Facility at beam lines ID22 and BM5, using monochromatic radiation in the range 15–17 KeV. With the experimental configuration selected, the x-ray camera used for the experiments[1,14] provides a field of view of about 1.4×1.4 mm^2, and nominal temporal and spatial resolutions down to about 0.15 s and 1.5 μm, respectively.

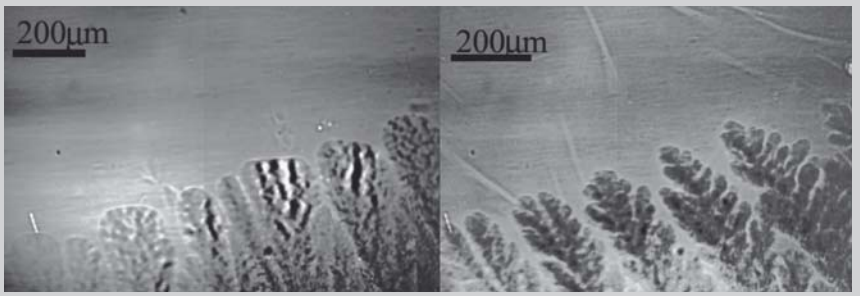

Figure 7. Cellular eutectic growth in Al-30Cu. G = 37.5 K/mm, v = 32 µm/s. *[See animation on-line.]*

there will, dependant upon the strength of the thermocapillarity, $\partial\sigma/\partial T$, be a certain droplet size regime where the Marangoni force supersedes the combination of gravity and Stokes friction. Thus, if the temperature gradient is adequately high, the bismuth droplets will be set in motion anitiparallel to **g,** and as they move toward higher temperature they may grow in size by coagulation or by accumulation of smaller, slower, or non-rising droplets. At the same time, the archetype shape of binodal lines in monotectic phase diagrams tells us that in equilibrium a gradual dissolution of the droplets would occur toward higher temperatures. Altogether there are now two possible outcomes for the droplet motion: coagulation and dissolution. Either the droplets grow large enough for gravity settlement to become dominant or they remain within a size regime where Marangoni motion is dominating.

In the first case there will be a coexistence of two flow regimes—Marangoni-driven upward flow of smaller droplets adjacent to settling flow initiated by gravity settlement of the larger droplets. In the shear between such flow regimes further flow-assisted coagulation will be promoted. For the droplets that remain within the Marangoni-dominated size regime, the droplets will normally move too fast to be completely dissolved at the binodal line, but transport into the miscible region where they finally dissolve and cause an unstable liquid density layering by bismuth supersaturation. Mesoscopic natural convection rolls arise with a diameter roughly similar to the length of the two-phase liquid region, here about 4 mm or 3.2 times the field of view.

In the presence of the mesoscopic convection, there will be settling transport of a bismuth-rich liquid that without new precipitation of bismuth droplets in the immiscibility gap can lead to a solutal undercooling of the monotectic reaction, for which cellular perturbations are amplified at the interface accompanied by a classical sinusoidal bismuth concentration profile. It can be seen from the video that Marangoni motion of droplets forming at the interface gives rise to microscopic convection rolls with roughly the same periodicity as the cells, and that droplet coagulation is prominent in the shear flow between the rolls. Furthermore the sequence reveals many intriguing details on short-scale droplet-droplet interaction and coagulation mechanisms, which can be compared with results from microscopic phase-field modeling,[30] showing the dominant role hydrodynamics have on coagulation in immiscible systems.

It should be noted that from the sequence shown in Figure 9 and more than 50 other sequences collected with

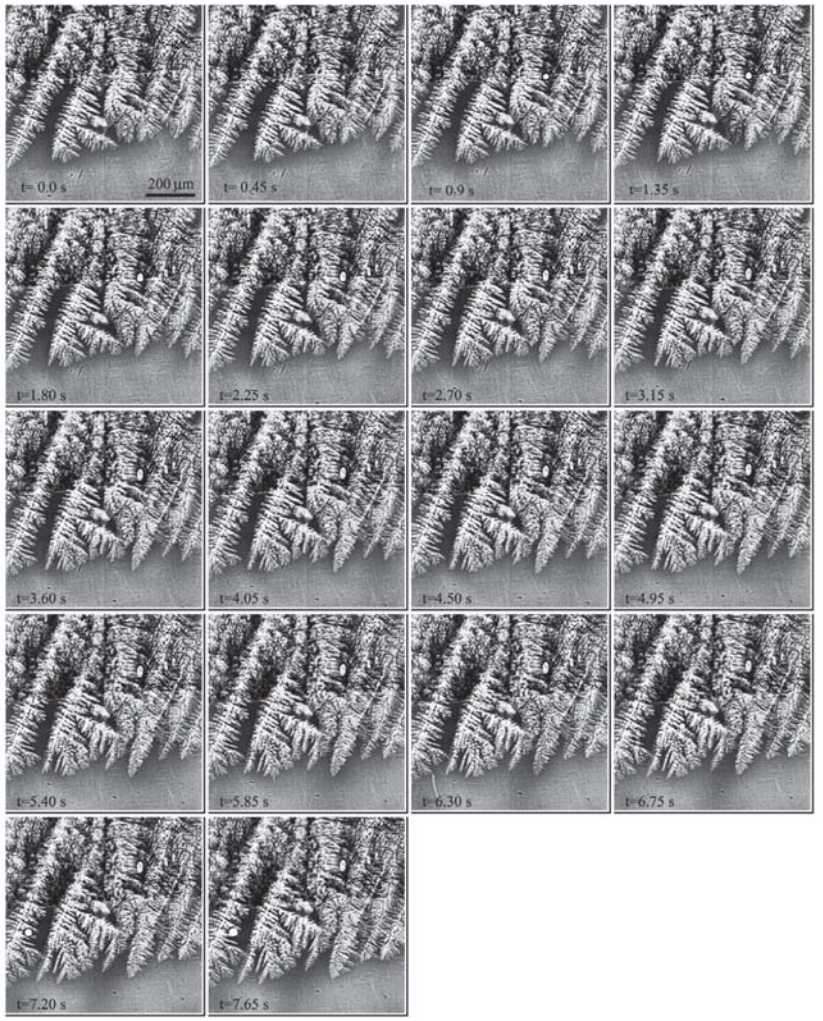

Figure 8. The formation of pores in Al-30Cu. Hydrogen gas bubbles are incorporated into the eutectic. G = 27 mm/s, v = 22.4 µm/s. *[See animation on-line.]*

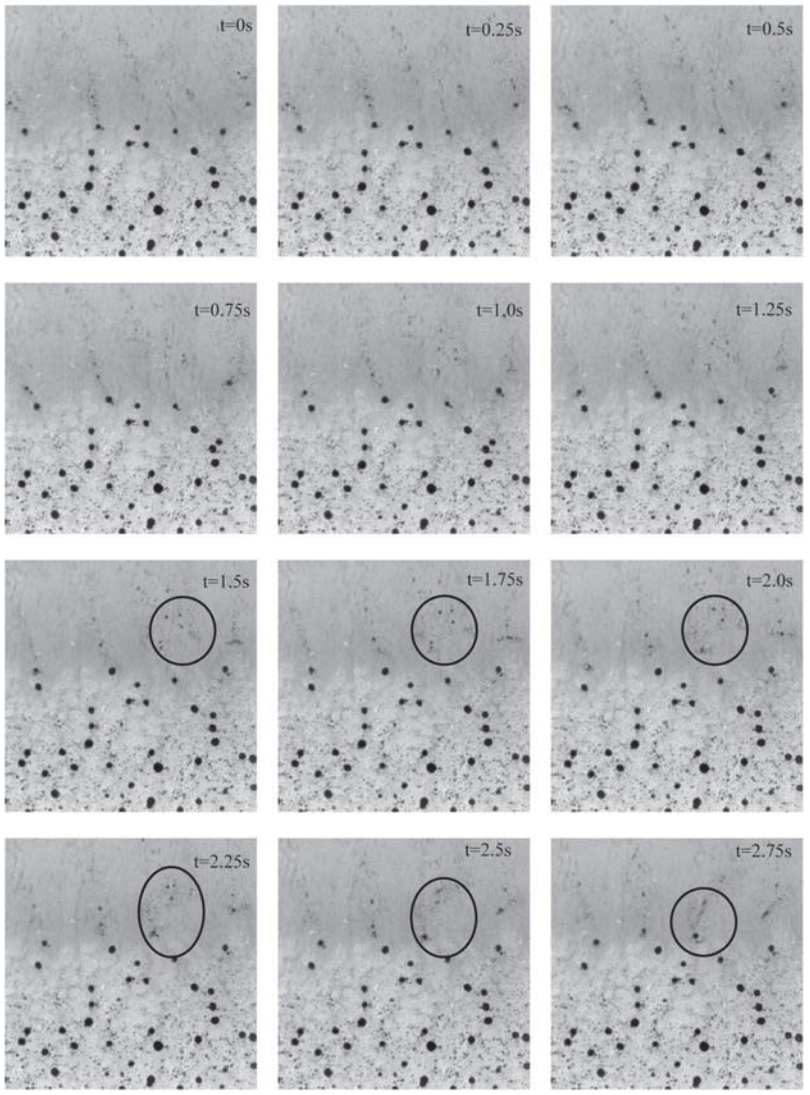

WEB

Figure 9. The liquid phase separation and monotectic reaction in an Al-6Bi alloy. G = 15 mm/s and v = 7.2 μm/s. *[See animation on-line.]*

different hypermonotectic Al-Bi constitutions, over a series of many samples, and for a large range of temperature gradients and pulling velocities, no observations could confirm nucleation of droplets in the immiscibility gap. In all sequences visible droplets appeared in the vicinity of the monotectic reaction, which potentially could be ascribed to a nucleation problem.

CONCLUSIONS

New techniques based on high intensity x-ray sources in combination with fast-read-out low-noise cameras have allowed in-situ imaging of alloy solidification with high spatial and temporal resolution. High-resolution images of solidification can provide quantitative data on solidification morphologies, solute distributions, and kinetics that will serve as benchmark data for modeling and for a better comprehension of solidification phenomena.

Video sequences of these techniques can be used in teaching to illustrate a wide range of alloy solidification phenomena.

ACKNOWLEDGEMENTS

The work reviewed has been sponsored by the Norwegian Research Council and Norwegian Industry through the NorLight program and by the European Space Agency through the ESA-MAP Monophas project. Prof. Frode Mo, Mr. Kjell Ramsøskar, and Dr. Paul Schaffer of NTNU and Dr. Anatoli Snigriev, ESRF, are acknowledged for important contributions to the work.

References

1. R.H. Mathiesen et al., *Met. Mat. Trans.,* 33B (2002), pp. 613–623.
2. J. Forsten and H. M. Miekkoaja, *J. Inst. Met.,* 99 (1971), p. 143.
3. M.P. Stephenson and J. Beech, *Proc. Intl. Conf. Solidification and Casting of Metals,* 18-21 (July 1977), pp. 34–36.
4. P.A. Curreri and W.F. Kaukler, *Met. & Mat. Trans.,* 27A (1996), pp. 801–808.
5. W.F. Kaukler, F. Rosenberger, and P.A. Curreri, *Met. Mat. Trans.,* 28A (1997), pp. 1705–1710.
6. J.N. Koster, *J. Min. Met. Mater.,* 49 (1997), pp. 31–35.
7. O. Ludwig et al., *Met. Mat. Trans.*, 36A (2005), pp. 1515–1523.
8. G. Grange et al., *J. Cryst. Growth,* 72 (1985), pp. 748–752.
9. T. Matsumiya et al., *Met. Mat. Trans.,* 18A (1987), pp. 723–727.
10. G. Grange et al., *Acta Mat.,* 45 (1997), pp. 2329–2338.
11. B. Billia et al., *Phys. Rev. Lett.,* 93 (2004), Art. no. 126105.
12. A. Snigirev et al., *Rev. Sci. Instr.*, 66 (1995), pp. 1–7.
13. R.H. Mathiesen et al., *Phys. Rev. Lett.,* 83 (1999), pp. 5062–5065.
14. J.-C. Labiche et al., *ESRF Newslett.,* 25 (1996), pp. 41–43.
15. R.H. Mathiesen and L. Arnberg, *Acta Mat.*, 53 (2005), pp. 947–956.
16. R.H. Mathiesen and L. Arnberg, *Mat. Sci. Forum,* 508 (2006), pp. 69–74.
17. R.H. Mathiesen and L. Arnberg, *Mat. Sci. Eng.*, A413-414 (2005), pp. 283–287.
18. H. Yasuda et al., *J. Cryst. Growth*, 262 (2004), pp. 645–652.
19. B. Li, H.D. Brody, and A. Kazimirov, *Phys. Rev.,* E70 (2004), Art. no. 062602.
20. B. Li, H.D. Brody, and A. Kazimorov, *Met. Mat. Trans.,* 37A (2006), pp. 1039–1044.
21. N. Mangelinck-Noel et al., *J. Phys. D: Appl. Phys.,* 38 (2005), pp. A28–A32.
22. G. Reinhardt et al., *Mat. Sci. Eng.*, A413 (2005), pp. 384–388.
23. T. Schenk et al., *J. Cryst. Growth,* 275 (2005), pp. 201–208.
24. M. Apel, H.J. Diepers, and I. Steinbach, *Proceedings of the Modeling, Welding and Advanced Solidification Processes–XI,* ed. C.-H. Gandin and M. Bellet (Warrendale, PA: TMS, 2006), pp. 505–511.
25. M. Rebow and D.J. Browne, *Scripta Mat.,* 56 (2007), pp. 481–484.
26. S. Boden et al., *Proc. of the 5th Decennial International Conference on Solidification Processing—SP07* (July 23–27, 2007, Sheffield, U.K.: 2007).
27. R.H. Mathiesen et al., *Met. Mat. Trans.,* 37A (2006), pp. 2515–2524.
28. D. Ruvalcaba et al., *Acta Mat.,* (2007), in press.
29. P.L. Schaffer, R.H. Mathiesen, and L. Arnberg, *Proceedings of the Modeling, Welding and Advanced Solidification Processes–XI,* ed. C.-H. Gandin and M. Bellet (Warrendale, PA: TMS, 2006), pp. 383–389.
30. G. Tegze, T. Pusztai, and L. Gránásy, *Mat. Sci. Eng.,* A413-414 (2005), pp. 418–422.

Lars Arnberg is with the Department of Materials Science and Engineering, Norwegian University of Science and Technology, Trondheim, Norway, and Ragnvald H. Mathiesen is with SINTEF Materials & Chemistry, Trondheim, Norway. Dr. Arnberg can be reached at lars.arnberg@material.ntnu.no.